Supplemental Material for C. T. Lao, J. Akroyd, N. Eaves, A. Smith, N. Morgan, A. Bhave, M. Kraft, "Modelling Particle Mass and Particle Number Emissions during the Active Regeneration of Diesel Particulate Filters", Proc. Combust. Inst. 37 (2019)

Table S1: Model input.

Parameter	Symbol	Value	Unit	Ref.
Inlet gas mass flow	$\dot{m}_{\mathrm{in}}$	586	kg/h	-
Particle mass flow	-	3.6	g/h	[5]
Inlet particle geometric mean diameter	-	38	nm	-
Inlet particle standard deviation	-	1.48	-	-
Inlet Oxygen mole fraction	$[O_2]_{\mathrm{in}}$	10	%	[8]
DPF length	-	304.8	mm	[5]
DPF diameter	-	304.8	mm	[5]
DPF cell density	-	200	cpsi	[5]
DPF wall thickness	L_{pw}	0.381	mm	-
DPF wall permeability	κ	1.22×10^{-13}	m^2	-
DPF wall porosity	ϵ_0	50	%	-
DPF wall pore diameter (320°C)	$d_{\mathrm{pore,ref}}$	13.1	μm	-
Soot packing density in wall	-	16	$\mathrm{kg/m}^3$	-
Percolation constant	ψ	0.87	-	-
Soot cake porosity	-	0.94	-	-
Soot cake primary particle diameter	-	15	nm	-
DPF heat capacity	C_{DPF}	15942	J/K	[25]
DPF thermal conductivity	λ	90	W/mK	[19]
DPF channel heat transfer coefficient	h_{conv}	129.3	$\mathrm{W/m}^2\mathrm{K}$	[26]
Axial discretisation	-	10	-	-
Wall discretisation	-	5	-	-
Regeneration rate pre-exponential factor	-	1.5×10^{24}	m/molKs	-
Regeneration activation energy	-	150	kJ/mol	[18]
Regeneration stoichiometric parameter	α	0.83	-	-
Pore expansion gradient	β	3.7×10^{-8}	m/K	-
Pore expansion reference temperature	T_{ref}	320	°C	[5]
Initial cake mass	m_{p0}	0.0679	kg	-
Soot cake filtration parameter 1	ω_1	150.0	-	-
Soot cake filtration parameter 2	ω_2	0.546	-	-

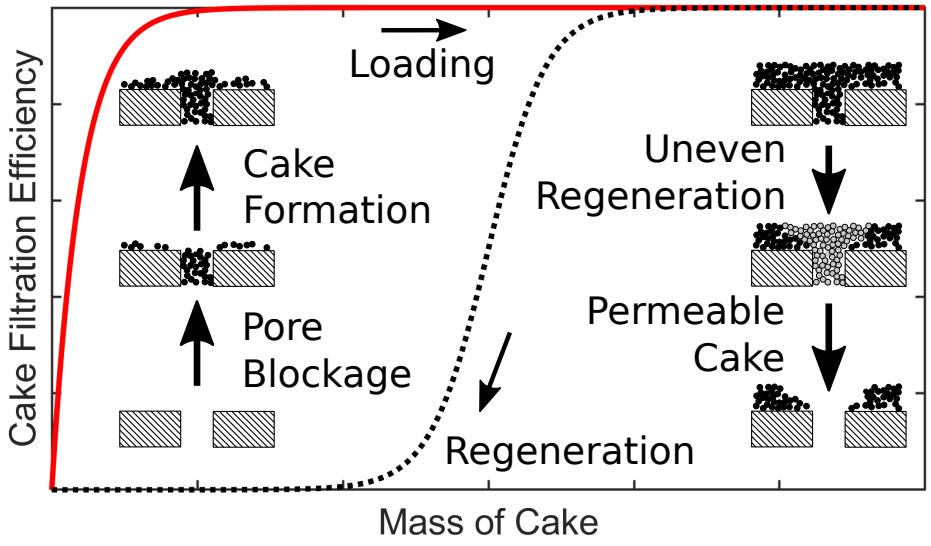

Figure S1: The filtration efficiency of the cake should exhibit a hysteretic behaviour during a load-regeneration cycle. The cake is no longer uniform during regeneration. Holes in the cake lead to decreased filtration efficiency despite significant cake mass remaining on the substrate of the wall.

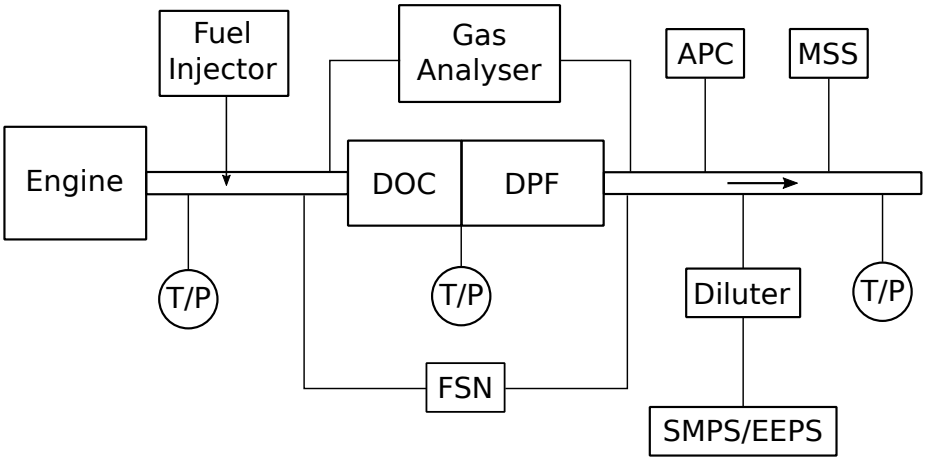

Figure S2: Experimental setup used by [5]. "T/P" indicates temperature and pressure measurements.

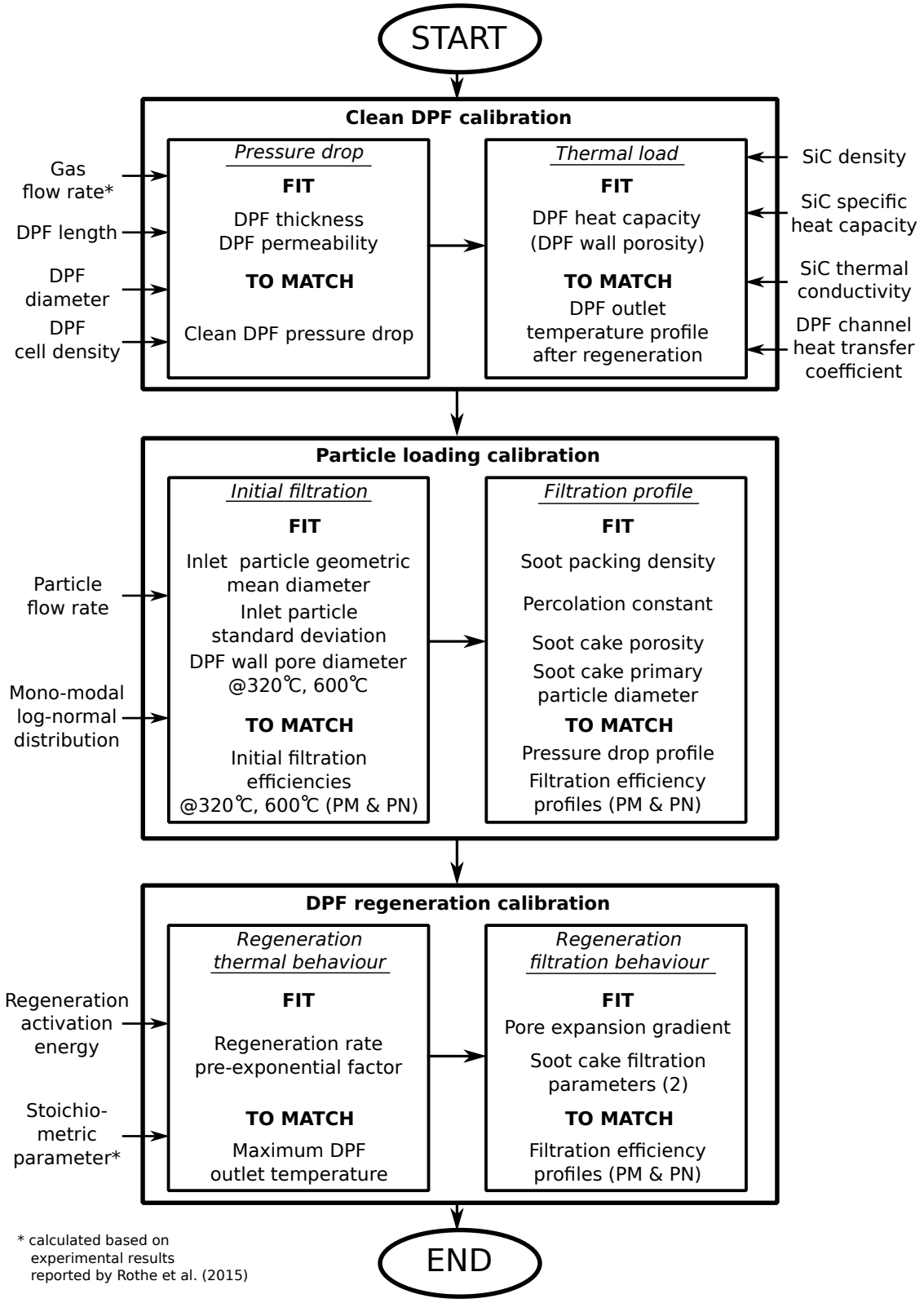

Figure S3: Block diagram for the calibration procedures. Once calibrated, the values of calibrated parameters are fixed for all subsequent parts of the calibration procedure.

Clean DPF calibration

Pressure drop

The length, diameter and cell density of the DPF are reported by Rothe et al. [5]. The gas flow-rate can be calculated from CO concentration, specific CO emission, engine speed and torque reported by Rothe et al. [5].

The thickness and the permeability of the wall of DPF is calibrated to match the pressure drop due to the clean DPF reported by Rothe et al. [5]. Since this problem is under-specified (calibrating two input variables to match one output variable), the resulting thickness and permeability are not unique. Their values are chosen such that they lie in typical ranges based on literature review [27] [28].

Thermal load

The thermal conductivity [19], specific heat capacity and density [25] of SiC are obtained from literature. The convective heat transfer coefficient between channel flow and the porous wall is calculated using the gas flow rate and correlation from Ramanathan et al. [26].

The overall heat capacity of the DPF is calibrated to match the DPF outlet temperature profile after regeneratiion has completed (where the DPF is clean). The porosity of the wall of the DPF can then be calculated from the calibrated overall heat capacity using the specific heat capacity and the density of SiC.

Particle loading calibration (Fig. 3)

Initial filtration

The particle flow rate is reported by Rothe et al. [5]. The inlet particle size distribution is assumed to be mono-modal log-normal, characterised by the geometric mean diameter and the standard deviation.

The filtration efficiency of the clean DPF is governed by the thickness, porosity and pore diameter of the porous wall, where the first two parameters have been calibrated. It is assumed in this study that the pore diameter would increase with temeprature due to expansion. Therefore it would take different values at 320°C, the temperature during particle loading, and 600°C, the temperature at the end of regeneration.

The geometric mean diameter and the standard deviation of the inlet particle size distribution, along with the pore diameter of the porous wall at two temperatures, are calibrated to match experimentally measured mass- and number-based filtration efficiency at the beginning of particle loading experiment and the end of active regeneration (where the DPF is clean).

Filtration profile

The soot packing density, percolation constant, soot cake porosity and soot cake primary particle diameter are calibrated to match the measured pressure drop profile and filtration efficiencies profiles (mass- and number-based) during the particle loading experiment. All four parameters affect the rate of pressure drop increase during transition between deep bed filtration and cake formation stage; the pressure drop profile during cake formation stage is controlled by soot cake porosity and soot cake primary particle diameter.

DPF regeneration calibration

Regeneration thermal behaviour (Fig. 4)

The activation energy of regeneration reaction is obtained from literature [18]. The stoichiometric parameter of the oxidation reaction is calculated from the ratio of CO and CO_2 produced from particles during TGA experiment performed by Rothe et al. [5].

The pre-exponential factor of regeneration reaction is calibrated to match the DPF outlet temperature profile during regeneration. In particular, it is noted that the pre-exponential factor has critical influence on the value and the timing of maximum DPF outlet temperature.

Regeneration filtration behaviour (Fig. 5)

The pore expansion gradient and the two soot cake filtration parameters are calibrated to match the mass- and number-based filtration efficiencies of the DPF during active regeneration.

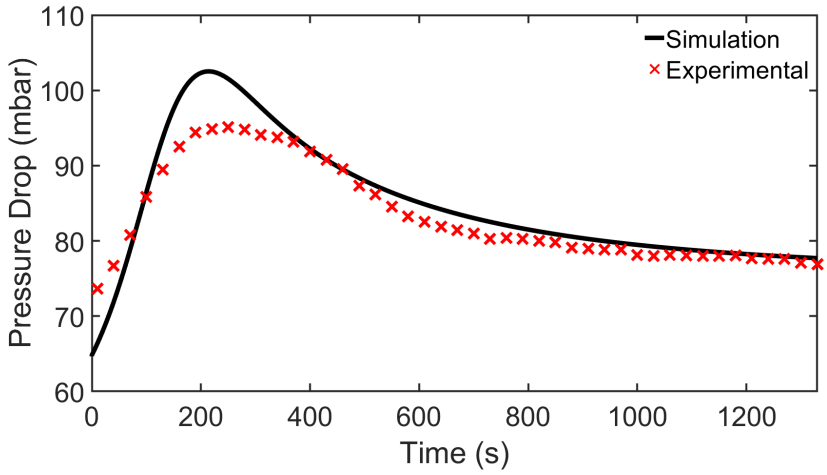

Figure S4: Comparison between experimentally measured and simulated pressure drop of the system during regeneration.

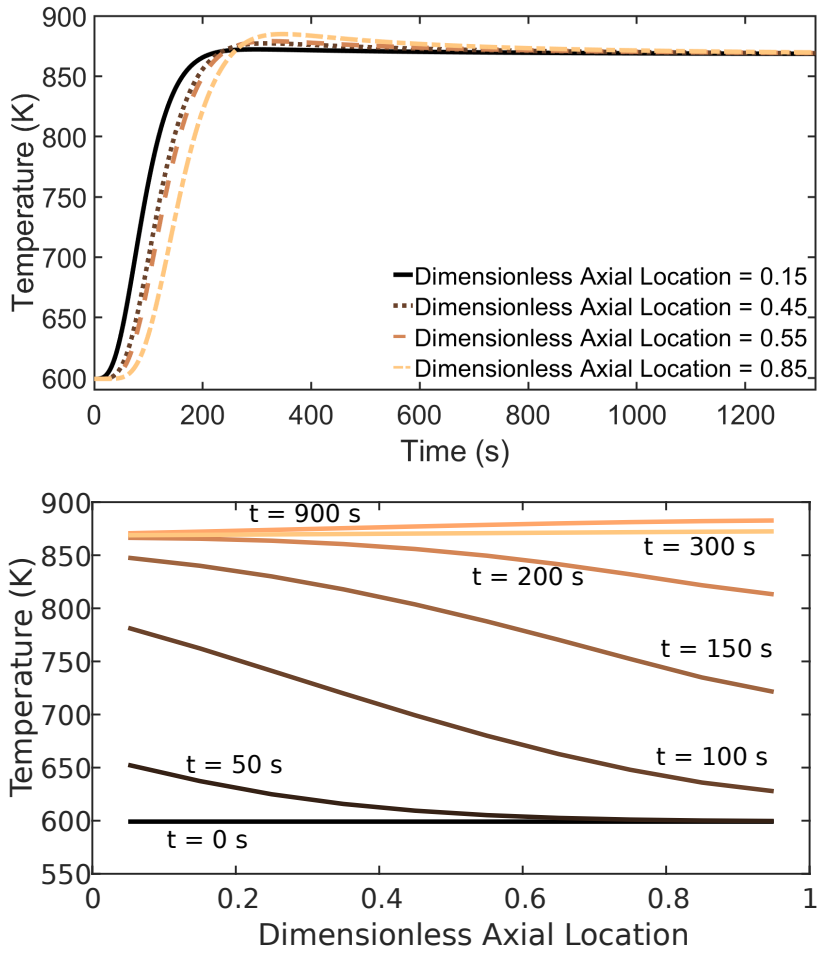

Figure S5: Simulated DPF wall temperature during regeneration.

References

[1] J. Lelieveld, J. S. Evans, M. Fnais, D. Giannadaki, A. Pozzer, Nature 525 (2015) 367–371.
[2] V. Ramanathan, G. Carmichael, Nat. Geosci. 1 (2008) 221–227.
[3] S. Bensaid, C. J. Caroca, N. Russo, D. Fino, Canadian Journal of Chemical Engineering 89 (2) (2011) 401–407.
[4] K. Yamamoto, Y. Kanamori, SAE Technical Paper 2015-01-1995 (2015).
[5] D. Rothe, M. Knauer, G. Emmerling, D. Deyerling, R. Niessner, Journal of Aerosol Science 90 (2015) 14–25.
[6] J. Ko, W. Si, D. Jin, C. Myung, S. Park, Journal of Aerosol Science 91 (2016) 62–77.
[7] S. Yoon, D. C. Quiros, H. A. Dwyer, J. F. Collins, M. Burnitzki, D. Chernich, J. D. Herner, Atmospheric Environment 122 (2015) 58–64.
[8] C. Beatrice, S. Di Iorio, C. Guido, P. Napolitano, Experimental Thermal and Fluid Science 39 (2012) 45–53.
[9] B. Guan, R. Zhan, H. Lin, Z. Huang, Journal of Environmental Management 154 (2015) 225–258.
[10] A. G. Konstandopoulos, M. Kostoglou, E. Skaperdas, E. Papaioannou, D. Zarvalis, E. Kladopoulou, SAE Technical Paper 2000-01-1016 (2000).
[11] M. Yu, D. Luss, V. Balakotaiah, Chemical Engineering Journal 232 (2013) 541–554.
[12] S. Yang, C. Deng, Y. Gao, Y. He, Advances in Mechanical Engineering 8 (3) (2016) 1–14.
[13] C. Beatrice, M. A. Costagliola, C. Guido, P. Napolitano, M. V. Prati, SAE Technical Paper 2017-24-0144 (2017).
[14] L. Sileghem, D. Bosteels, J. May, C. Favre, S. Verhelst, Transportation Research Part D 32 (2014) 70–85.
[15] C. Depcik, D. Assanis, Journal of Engineering for Gas Turbines and Power 130 (6) (2008) 062807-1–062807-18.
[16] O. A. Haralampous, G. C. Koltsakis, AIChE Journal 50 (9) (2004) 2008–2019.
[17] I. P. Kandylas, G. C. Koltsakis, Industrial and Engineering Chemistry Research 41 (9) (2002) 2115–2123.
[18] E. A. Kladopoulou, S. L. Yang, J. H. Johnson, G. G. Parker, A. G. Konstandopoulos, SAE Technical Paper 2003-01-0842 (2003).
[19] C. Benaqqa, M. Gomina, A. Beurotte, M. Boussuge, B. Delattre, K. Pajot, E. Pawlak, F. Rodrigues, Applied Thermal Engineering 62 (2014) 599–606.
[20] J. Gong, C. J. Rutland, Environmental Science and Technology 49 (8) (2015) 4963–4970.
[21] A. G. Konstandopoulos, E. Skaperdas, M. Masoudi, SAE Technical Paper 2002-01-1015 (2002).
[22] E. Cauda, S. Hernandez, D. Fino, G. Saracco, V. Specchia, Environmental and Science Technology 40 (2006) 5532–5537.
[23] S. Choi, K. Oh, C. Lee, Energy 77 (2014) 327–337.
[24] S. J. Harris, M. Maricq, Aerosol Science 32 (2001) 749–764.
[25] N. M. Ghoniem, Journal of Nuclear Materials 191-194 (1992) 515–519.
[26] K. Ramanathan, V. Balakotaiah, D. H. West, Chemical Engineering Science 58 (2003) 1381–1405.
[27] S. Bensaid, D. L. Marchisio, D. Fino, G. Saracco, V. Specchia, Chemical Engineering Journal 154 (2009) 211–218.
[28] J. E, L. Xie, Q. Zuo, G. Zhang, Atmospheric Pollution Research 7 (2016) 9–17.
[29] C. T. Lao, J. Akroyd, N. Eaves, A. Smith, N. Morgan, A. Bhave, M. Kraft, “Modelling Particle Mass and Particle Number Emissions during the Active Regeneration of Diesel Particulate Filters”, Proc. Combust. Inst. 37 (2019)